ADVANCED ELECTRONIC MATERIALS
Open Access
www.advelectronicmat.de

Kinetics and Physicochemical Characteristics of Electrodeposited PEDOT:PSS Thin Film Growth

*Hajar Mousavi, Laura M Ferrari, Amelia Whiteley, and Esma Ismailova**

In bioelectronics, conducting polymer coatings allow the reduction of the impedance of metallic electrodes and facilitate the translation of bioelectrical signals at their interface. Such coatings can be made using thin film deposition from a solution or direct synthesis via electrodeposition. The electrical control over the deposition offers the possibility for a fine-tuning of the film's thickness and structure. However, the mechanical stability of such coatings mainly suffer from their poor adhesion to the electrode surface and film cracking. Here, an extended study on the kinetics of poly(3,4-ethylene dioxythiophene):poly(styrenesulfonate) (PEDOT:PSS) electropolymerization and the evolution of its physicochemical properties is provided. The impedance spectroscopy closely follows the electrochemical variations during the PEDOT:PSS's film growth, described by modeled equivalent circuits. The film's properties change during polymerization in relation to the supporting electrode size, its surface chemistry, and the deposition time. The film growth structures polymeric morphology in a confluent layer with a strong thickness increase before reaching its mechanical surface failure. Before this point, the film remains stable over a hundred cycles of applied potential strain in a defined redox window. These evaluations benchmark the PEDOT:PSS film properties during its electropolymerization toward electrochemically tunable transducers for bioelectronics.

1. Introduction

Bioelectronic devices based on organic electronic materials have emerged in recent years demonstrating a steadfast potential for technology transfer.[1] Three main families of devices stand out for their application in in vitro, in vivo, and on-body diagnostics. microelectrode arrays (MEAs) in junction with cell tissue are able to detect the presence of pathogens, toxins or follow the development of pharmacological action on a biological model such as BBB (blood brain barrier) or cancer cells.[2] Implantable probes made with organics also show an outstanding biomechanical compatibility with biological tissue and an advanced detection of electrophysiological activities.[3,4] Similar improvements in signal quality detection are seen in wearables made of conductive polymers when combined with textiles, paper, and flexible substrates.[5–7] In all these applications, long-term performance of the devices and materials functionality are important parameters that need to be characterized while developing novel bioelectronics technologies.

In the past few decades, conductive polymers (CPs) have been extensively used to enhance the characteristics of traditional metallic microelectrodes in bioelectronics.[1,8,9] Their coupled ionic/electronic mixed conductivity is particularly interesting at the interface with an ionically conductive living tissue allowing for a precise signal transduction.[10–14] This is extremely valuable for microelectrode arrays as they provide high spatial resolution in monitoring of living tissues, as their impedances scale up by several orders of magnitude in comparison with macrosized electrodes. The main advantage of coating metal-based electrodes with conductive

H. Mousavi, E. Ismailova, A. Whitely
Mines Saint-Etienne
Centre CMP
Department of BEL
Gardanne F-13541, France
E-mail: ismailova@emse.fr

L. M. Ferrari
INRIA
Université Côte d'Azur
Sophia Antipolis 06902, France

A. Whiteley
University of Grenoble Alpes
CEA
Leti 38000, France

The ORCID identification number(s) for the author(s) of this article can be found under https://doi.org/10.1002/aelm.202201282.

DOI: 10.1002/aelm.202201282

polymers is that they reduce the impedance by increasing the capacitance of the electrode at the interface thanks to volumetric charge transfer capability of CPs.[13,15–18] There is a trade-off between the resolution and quality of the signal as the signal-to-noise ratio drops significantly with increase of impedance.[13,19]

While using electrochemical impedance spectroscopy (EIS) to study the CP-coated electrode's interfacial properties, their combined capacitive and resistive behaviors lead to the occurrence of a cut-off frequency as a key figure of merit when comparing with metallic electrodes. It is defined as the frequency at which the signal power reduces to its half magnitude.[15] In the Bode representation of impedance, it corresponds to the 45° phase, where the electrodes transit from predominantly resistive to predominantly capacitive. At this point, the impedance increases by several orders of magnitude. As result, the signals above the cut-off frequency can be recorded accurately, while low frequency signals are phase-shifted, filtered, and eventually undergo nonlinear distortion.[15,16,20,21] In this regard, biological signals span in a broad frequency range, from as low as 1 Hz to as high as 1 kHz.[22] As MEAs have a high cut-off frequency (<10 kHz),[15] the conductive polymer coatings push this frequency to lower values avoiding signals disturbance during their recordings. Such phenomenon is known to depend on volumetric charge transfer of the conducting polymers that delays the double-layer capacitance creation at low frequencies (>0.1 kHz).[15,23–26]

Among conductive polymers, poly(3,4-ethylenedioxythiophene):poly(styrenesulfonate) (PEDOT:PSS) is the most successful material thanks to its biocompatibility, high charge capacity, chemical stability, and commercial availability.[27,28] It can be easily electropolymerized onto different electrode surfaces. The polymerization starts with an oxidation of 3,4-ethylene dioxythiophene (EDOT) monomer resulting in positively charged chains.[29–31] As the resulting PEDOT is a semiconductive polymer, the introduction of additional counter ions form an electrostatically stable and conductive structure at the backbone. Among the possible counter ions, negatively charged poly(sodium 4-styrenesulfonate) (NaPSS) together with PEDOT form the most successful combination because of their high electrochemical stability (during oxidation/reduction processes), good film-forming properties, and resulting high conductivity.[27,28,30–32] For the first time, Yamoto et al. reported the electropolymerization of PEDOT:PSS.[33,34] Afterward, the morphology, mechanical properties, and conductivity of PEDOT:PSS films have been largely studied in various deposition conditions highlighting that deposition technique affects the film properties.[27] For example, Khan et al. showed that during electrodeposition the maximum polymer growth happens at the edge of the electrode due to the potential gradient over the electrode's surface. Some claims in the literature stipulate that galvanostatic technique results in a better coating uniformity.[35] Castagnola et al. underlined that electropolymerized PEDOT film morphology varies with cyclic voltammetry (CV) scan rate, the EDOT monomer concentration, and the current density.[36] They also showed that the CV produces a uniform film, while galvanostatic and potentiostatic depositions create large island aggregates.[37] Cui et al. showed that PEDOT:PSS film has an open fuzzy structure that allows fast ion transport across the film, regardless of deposition technique.[38] Based on the literature above, there is not enough consistent data allowing for a clear benchmark in PEDOT:PSS synthesis while using electropolymerization. This can be explained by the presence of limiting factors occurring during the film growth or initiating from the electrodes with different surface properties, resulting in a multiparametric complexity understanding of the process.

A poor mechanical stability during electropolymerization of PEDOT:PSS has been revealed in the literature. Its attachment to the substrate depends on its thickness, adhesion surface properties, and electrodeposition-operating parameters (applied voltage/current, duration and repetition). For example, it develops cracks and delamination upon mechanical deformation, sterilization procedure, and in charge injection applications[39–41] limiting coating's long-term performances. Therefore, some strategies have been proposed to promote PEDOT:PSS adhesion to the metallic electrodes. Qu et al. characterized the stiffness and adhesion of electrodeposited PEDOT:PSS on metal electrodes.[41] They measured interfacial shear strength which showed the linear relationship between PEDOT:PSS thickness and cracks spacing.[42] As solution, the polymer–substrate adhesion can be promoted by modifying the electrode's surface. Nanostructured platinum with iridium oxide improves the PEDOT:PSS adhesion through the roughening of the electrode's surface.[43] From the chemical point, EDOT derivatives such as EDOT-NH_2 and EDOT-acid boost the mechanical stability of the polymerized films by forming a chemical link between the electrode and the film.[41,44]

In addition, there is a growing interest in lowering the electrode's impedance for biomedical applications, and carbon-based electrodes showed great potential due to their softness, flexible manufacturing, compatibility with diagnostic imaging and extensive possibility of biofunctionalization. Welle et al. electropolymerized PEDOT:pTS (sodium *p*-toluene sulfonate) on carbon microfibers for deep brain implantation.[45] Taylor et al. electrodeposited PEDOT/CNT on carbon microfibers for dopamine sensing.[46] Yang et al. electropolymerized PEDOT:PSS on glassy carbon to monitor tricresyl phosphate.[47] Nevertheless, the understanding of PEDOT:PSS polymerization, and its properties evolution on organic substrates is missing due to the limited studies on the subject.

Here, we present the electropolymerization of PEDOT film doped with PSS on three of the most representative substrates: gold macroelectrodes (m-Au), gold microwires (μ-Au), and carbon microwires (μ-C) with potentiostatic, galvanostatic, and CV techniques. This study empirically evaluates the key parameters influencing the PEDOT:PSS film properties between deposition techniques and substrate characteristics. First, we study the kinetics of the polymerization by looking at the PEDOT:PSS thin film growth on the surface of m-Au electrodes coated with the potentiostatic technique where the applied voltage is independent of electrode's size and scan speed potential. The study of chemical structure together with the conductivity at different thicknesses evaluates the electrical properties changes of the growing film during the polymerization. The morphology of polymer film, its stability and interface impedance are assessed as a factor of the substrate type and deposition technique using electrochemical impedance and light spectroscopies, as well as optical and electron microscopies. We show that the film

cracking appears in relation to the substrate size and nature while reaching several micrometers thickness. The impedance evaluations of all the three types of electrodes follow the PEDOT:PSS film growth kinetics during the electropolymerization. Finally, after defining the optimized deposition conditions, the cycled CV follows the electrochemical stability of the PEDOT:PSS films. These results show that only a very thin film of PEDOT:PSS is required to electrochemically enhance the electrical properties of each type of coated electrode. Therefore, the understanding of the growing kinetics of CPs during electrodeposition process enables to controllably modify and tune the electrodes mixed conducting performances toward bioelectronics applications dealing with frequency dependent biosignals.

2. Results and Discussion

2.1. PEDOT:PSS Electropolymerization versus Structural Characteristics

PEDOT:PSS electropolymerization happens by oxidation of EDOT monomers under an applied current or voltage which creates protonated intermediate radicals. Two activated monomers combine together and create two protons letting PEDOT positively charged chains to emerge (see Figure S1, Supporting Information).[48] The polymerization in the presence of negatively charged PSS serves as a counter anion to compensate $PEDOT^+$ charges by forming an electrostatically stable bipolymer thin film on the electrode surface, as schematically shown in **Figure 1**a. Such molecular doping allows for electron transfer by creating an electrically conducting film. To follow the structural evolution of the growing film, we first characterized its chemical composition and thickness as a function of the deposition time. For this, standard round-shaped m-Au electrodes are coated with PEDOT:PSS to allow for polymerized film's characterization. The electropolymerization using the potentiostatic technique was timed at 5, 10, 50, 100, and 200 s intervals at 1.1 V. The potential was set to avoid water hydrolysis during electropolymerization. The combined scanning electron microscopy (SEM) and energy-dispersive X-ray (EDX) imaging of resulting electrodes quantifies the synthetically reacted PEDOT and PSS chains by tracking the evolution of the sulfur (S) element over the polymerization (Figure 1b). The sulfur percentage increased gradually from 2.4% at 5 s to 33.5% at 50 s against the gold content. As seen in the lateral electrode's surface inspection by SEM, at a very early stage, the PEDOT:PSS covers entirely the m-Au electrodes. In galvanostatic and CV methods, the sulfur ratio increases from 2.3% to 22.7% (5 to 50 s) and 1.4% to 17.2% (1–5 scans), respectively. Therefore, the results of the potentiostatic method compared to the galvanostatic show a slightly higher sulfur content addition, 33.5% against 22.7% at 50 s. The CV data are difficult to correlate as the method is based on the cyclic reduction and oxidation processes and the kinetics of the sulfur content growth should be much slower as confirmed by the results.

Figure 1c shows an optical view of the PEDOT:PSS electrode that has been delaminated from the m-Au after 200 s of polymerization using polyvinyl alcohol (PVA) support. SEM cross-sectional imaging of individual electrodes defines the PEDOT:PSS's

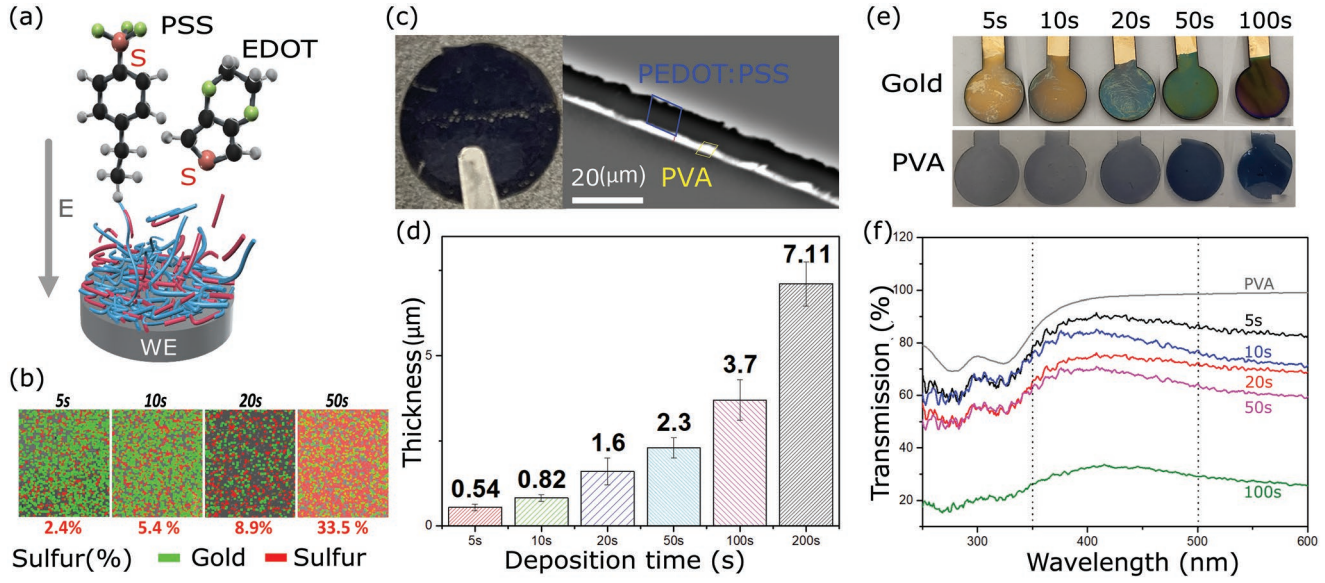

Figure 1. The kinetics of PEDOT:PSS growth during electropolymerization: a) schematic illustration of PEDOT:PSS electropolymerization showing the electrode (WE), the chemical structure of the main molecules participating the electropolymerization and the direction of the electrical field. b) Energy dispersive X-ray (EDX) imaging of PEDOT:PSS-coated m-Au electrodes. The images represent gold and sulfur percentages upon increasing polymerization time. The green color represents gold and the red represents sulfur contents in 10 × 10 μm images. c) The optical top view and scanning electron microscopy cross-section images of PEDOT:PSS/PVA film after 200 s deposition. d) The thickness measurements of PEDOT:PSS film evolution at various deposition times. The used electrode diameter is 1 cm. e) Optical images of PEDOT:PSS film growth at different deposition times on gold and after their peeling off using PVA layer. f) UV–vis transmission spectra of PEDOT:PSS films at different deposition times on PVA, including pristine PVA film spectrum.

ADVANCED ELECTRONIC MATERIALS
Open Access
www.advelectronicmat.de

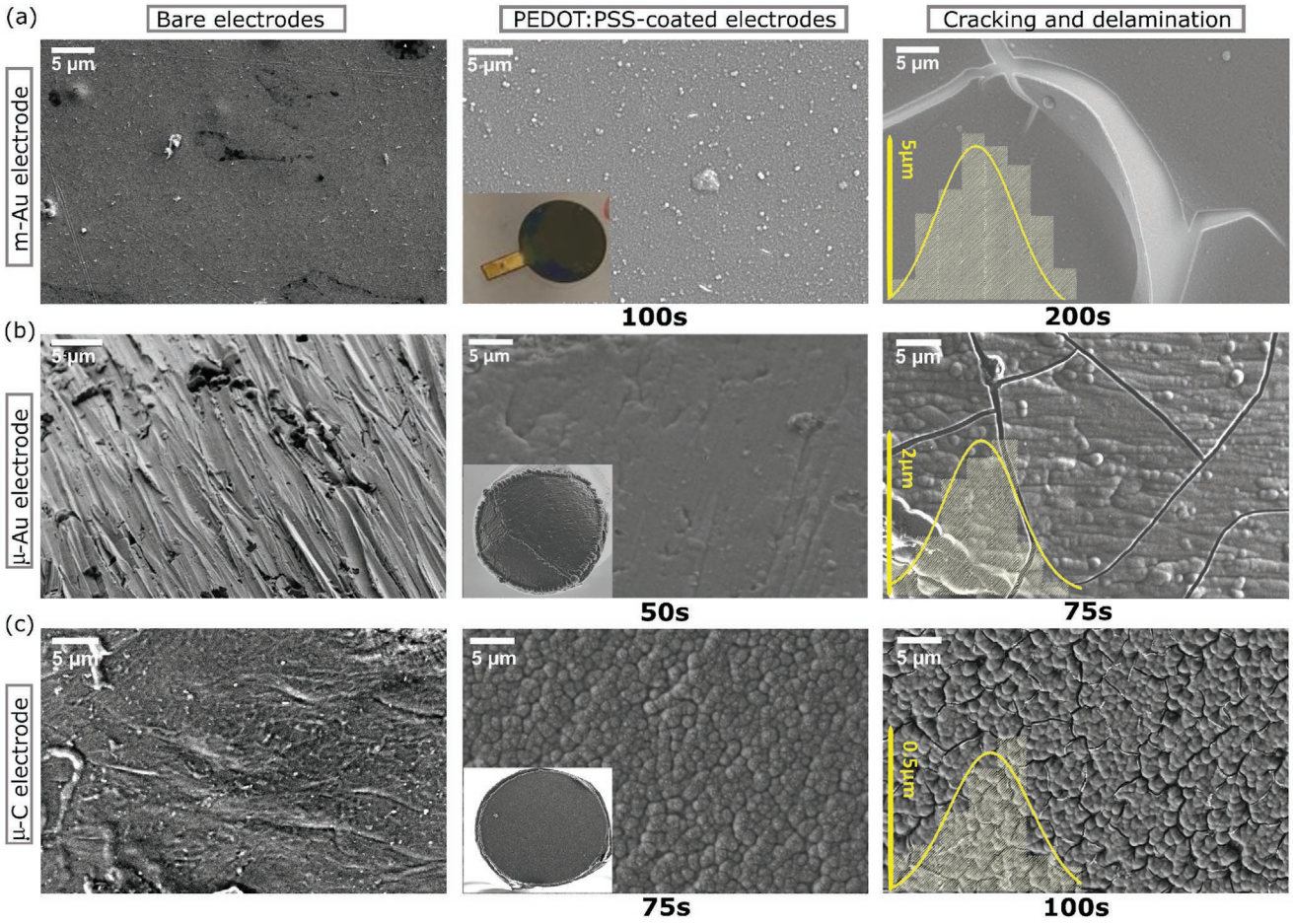

Figure 2. Structural growth of PEDOT:PSS film during potentiostatic deposition on three electrodes. SEM micrographs of a) m-Au electrode: bare (left), PEDOT:PSS-coated after 100s (middle, the inset shows an optical image of the electrode with dark blue PEDOT:PSS coating in the circular area with 1 cm diameter) and the cracks formation after 200 s (right, the inset represents the cracks distribution by size over the electrode surface). b) µ-Au electrode: bare (left), PEDOT:PSS-coated after 50 s (middle) (the inset shows the electrode surface after the coating with 125 µm diameter) and the cracks appearance already at 75 s (right) (the inset shows the cracks distribution). c) µ-C electrode: bare (left), PEDOT:PSS-coated after 75 s (middle) (the inset shows the electrode surface after the coating with 400 µm diameter) and the cracks appearance after 100 s (right) (the inset shows the cracks distribution).

thicknesses evolution over different deposition intervals. As illustrated in **Figure 2**d, after 5 s of deposition the film thickness reaches 540 ± 10 nm and after 200 s is 7.11 ± 0.6 µm. Such progressive thickness increase as a function of deposition time follows the same observations reported by SEM-EDX evaluations of S percentage (Figure 1b). Thickness of PEDOT:PSS in galvanostatic deposition is between 360 ± 80 nm and 5.4 ± 0.850 µm for 5–200 s. In the CV method, they change between 120 ± 50 nm and 3.8 ± 0.890 µm at 1–5 scans of deposition.

In comparison, Castagnola et al.[37] reported a thickness of 556 nm upon 10 s of deposition (on gold–polyamide substrate) using an EDOT to NaPSS ratio of 1:7 (w:w) and the same voltage of 1.1 V. However, Wustunit et al. reported a thickness of 320 nm for duration of 300 s using EDOT:NaPSS ratio of 1:8 (w:w) at 1 V deposition on gold–polyamide substrates.[49] In both studies, the ratio of EDOT to NaPSS was lower than in our experiment [1:14 (w:w)]. Cui et al. electropolymerized PEDOT:PSS on gold-coated silicon probes, with the same EDOT:NaPSS ratio, and thickness between 1 and 4 µm by adopting the deposition time at the constant voltage of 1.1 V.[38] This is comparable with our results. These variations in the film growth kinetics over the same technique of deposition highlight the importance of the applied voltage and the EDOT:NaPSS ratio on the resulting film characteristics. Therefore, potentiostatic electropolymerization rate and subsequently the film thickness are highly affected by the applied voltage.

Following the thickness evaluation, the electrical conductivity of the PEDOT:PSS films on electrically neutral PVA is calculated with a four-point probe measurement using the same samples. Conductivities of 117 ± 0.002, 97 ± 0.01, 83 ± 0.007, 125 ± 0.004, and 112 ± 0.003 S cm^{-1} were measured for 5, 10, 20, 50, and 100 s of electrodeposition, respectively. As presented in the literature, the PEDOT:PSS's electrical conductivity of blends varies from 0.01 to 4600 S cm^{-1}. The conductivity can be altered by adding glycerol, dodecyl benzene sulfonic acid, perichloric acid,[50] and (3-glycidyloxypropyl) trimethoxy silane allowing for conformational changes between PEDOT and PSS by promoting the creation of conductive domains.[25] Modaressi and Zozoulenko modeled the impact of a solvent treatment on PEDOT:PSS film conductivity through PEDO-rich

areas containing PEDOT and PSS chains (conductive domains) and PSS-rich areas composed of PSSH chains (insulating domains) using molecular dynamics simulation. Therefore, the solvent treatment deprotonates PSS chains and improves the film conductivity.[51] Castagnola et al. reported the conductivity of electrodeposited PEDOT:PSS films between 30 and 120 S cm^{-1} depending on the deposition parameters.[37] In our case, the film's electrical properties seem to not change during the deposition using the potentiostatic technique. In galvanostatic polymerization, the electrical conductivity are 91 ± 0.001, 78 ± 0.003, 101 ± 0.006, 118 ± 0.002, and 98 ± 0.005 S cm^{-1} for 5, 10, 20, 50, and 100 s, respectively. Those obtained by CV technique are 87 ± 0.002, 98 ± 0.005, and 103 ± 0.007 for 1, 2, and 5 scans, respectively. This indicates that PEDOT and PSS chains build up in the film without significant change during deposition.

The UV–vis spectroscopy provides information on the oxidation state of conductive polymers. It reveals the doping level of the positively charged polymer by the counterions which determines the electrical conductivity of the film.[52,53] Thanks to the PVA's high transparency, the PEDOT:PSS's intrinsic optical properties could be determined at different times of electropolymerization. Here, upon the growth of PEDOT:PSS, the optical images show a reduction of the film's transparency and a spectral transition from light to dark blue (Figure 1e). UV–vis spectroscopy of PEDOT:PSS film on PVA shows a large absorption peak between 350 and 500 nm at various thicknesses with a slight shift in wavelength for longer polymerizations (100 s) (Figure 1f). Since PVA's transmission remains 100% in this window, only the contribution of the PEDOT:PSS's transmission percentage decreases with increasing deposition time. This suggests that the ratio of PEDOT:PSS remains constant and the overall doping level does not change during the synthesis. In addition, the attenuated total reflectance–Fourier transform infrared (ATR-FTIR) (Figure S2, Supporting Information) and Raman spectrum analysis (Figure S3, Supporting Information) support these observations. ATR-FTIR reveals the presence of the PEDOT's asymmetric C=C stretches of the thiophene ring at 1515 cm^{-1} and a peak around 978 cm^{-1} that refers to the C−S−C bond. This confirms a successful polymerization of EDOT monomers. The presence of PSS's bands appear at around 1178 cm^{-1} (S=O band), 1136 cm^{-1} (SO_3H group), and 1475 cm^{-1} (C−C of aromatic ring). The intensity ratio between each representative peak does not change along the deposition, as previously reported.[54,55] The peaks' amplitude rises with the deposition time. Raman spectrum provides detailed information about the structural transformation of PEDOT according to the doping level. The most significant shift due to the PEDOT:PSS ratio variation occurs at the symmetric Cα=Cβ stretching band at 1438 cm^{-1}. In our case, it remains unchanged during the polymerization. Other noticeable peaks at 1599 cm^{-1} (Cα=Cβ stretching band), 1370 cm^{-1} (Cβ=Cβ), and 1252 cm^{-1} (Cα=Cα') stretching bands do not change.[56,57] These results support that PEDOT to PSS ratio remains similar as a function of the film thickness.

2.2. Electropolymerized PEDOT:PSS Film Characteristics

Since electropolymerization requires a conductive surface to begin, we evaluated the impact of the substrate's type on the morphology of growing PEDOT:PSS film and its adhesion. We observed considerable morphological variations of the film according to the substrate type. Indeed, on m-Au and μ-Au electrodes, the PEDOT:PSS forms a flat film (Figure 2a left and middle, Figure 2b left and middle), whereas a structured cauliflower shape appears on μ-C electrodes (Figure 2c left and middle) during potentiostatic deposition. Several studies show that the CV technique creates a uniform film while potentiostatic and galvanostatic techniques tend to create PEDOT:PSS islands due to the nonuniform current distribution.[27,37,38] In our experiments on three different types of electrodes, we do not see any changes in the morphology of the PEDOT:PSS as function of electropolymerization technique (Figures S4 and S5, Supporting Information) rather than as function of the electrode type.

The extensive growth of PEDOT:PSS leads to its cracking and delamination from the electrode surface because of its weak adhesion forces and absence of any chemical interaction with the substrate.[41,42,44,58–59] Indeed, we measured the adhesion force using a peel-off technique that indicated a value of 300 ± 100 mN for different coatings on m-Au electrodes before the appearance of cracks (see Figure S6, Supporting Information). As the film grows, the mechanical tension over the electrodes' surface first results in small cracks, which then grow and cause a substantial film self-delamination. The cracks formation starts at 200, 100, and 75 s on m-Au, μ-Au, and μ-C electrodes, respectively (Figure 2a, right, Figure 2b, right, and Figure 2c, right). They tend to form later on larger electrodes. However, the morphology of film cracking changes according to the substrate. μ-C electrodes show smaller cracks (Figure 2c, right) with their width distribution between 0.18 and 0.35 μm. The cracks get thicker on the μ-Au electrode where the width varies between 0.55 and 1.54 μm (Figure 2b, right). In the case of m-Au, the delamination occurs nearly at the same time as the cracking. The crack's width ranges from 1.8 to 5.4 μm (Figure 2a, right). The size and time window of cracking and delamination correlates to the PEDOT:PSS adhesion and electrode's surface properties. The cracking happens much earlier on μ-Au electrodes than on m-Au whereas their sizes are in the μm scale. The faster appearance time can be explained by the potential distribution which is higher over the smaller surface areas. The higher cracking and delamination in m-Au electrodes is observed because of the bigger surface tension produced at the cracking point. Though, the consequence of the PEDOT:PSS attachment to the electrode can be observed on two different μ-electrodes. The difference between μ-Au and μ-C is in their chemical surface nature. μ-C compared to the Au has lower electrical conductivity due to its organic nature. This allows for a stronger PEDOT:PSS attachment as cracking starts later in μ-C and their distribution is almost three times lower compared to the μ-Au. Therefore, this is not sufficient to avoid mechanical degradation of PEDOT:PSS films. Increasing the surface roughness has been previously applied as a successful strategy to improve PEDOT:PSS's adhesion to the metallic substrates. For example, Boheler et al. used nanostructured platinum and iridium oxide (IrOx) as adhesion promoters to mechanically anchor polymers.[58–60] Chemical functionalization of EDOT monomers with adhesion promoting side groups showed better results in mechanical satiability of electropolymerized films.[41,44]

ADVANCED ELECTRONIC MATERIALS
Open Access
www.advelectronicmat.de

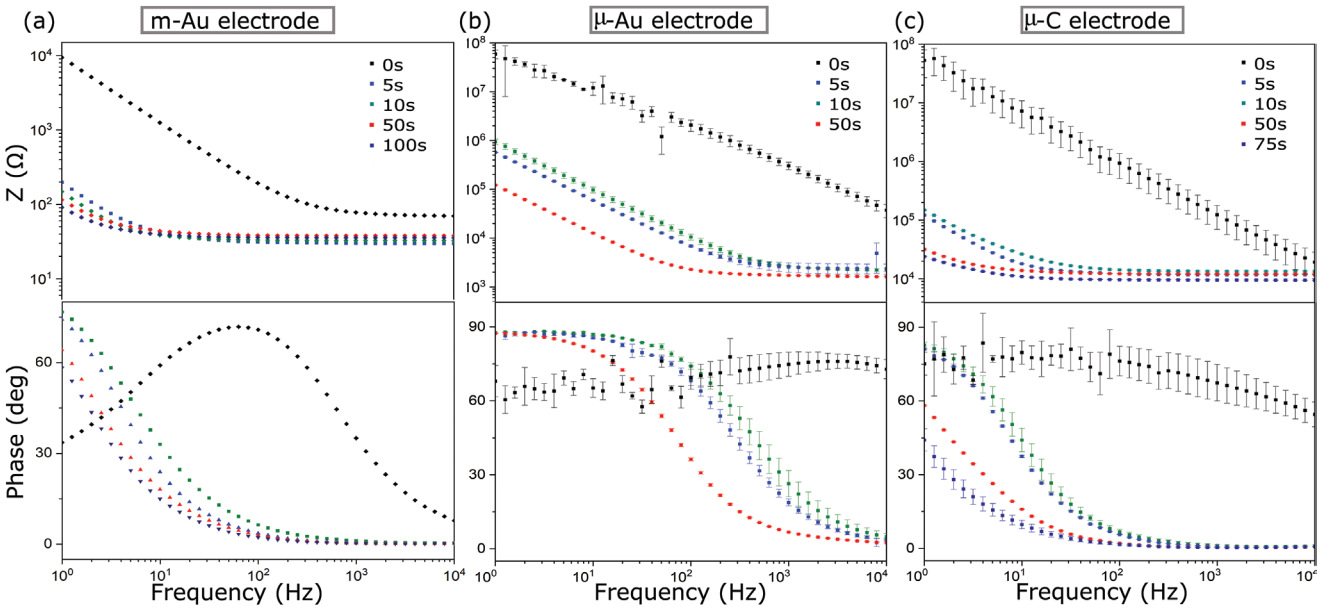

Figure 3. Electrochemical impedance spectroscopy: a) Bode plot, magnitude (logarithmic) and phase (linear), of m-Au, b) μ-Au and c) μ-C electrodes coated with PEDOT: PSS via potentiostatic technique (1.1 V vs Ag/AgCl) at different times are shown. The curves show dynamic variation of electrochemical behavior of electrodes during the coating.

2.3. Electrochemical Characteristics of Electropolymerized PEDOT:PSS

The electrochemical impedance spectroscopy (EIS) evaluations of m-Au, μ-Au, and μ-C electrodes are represented as a function of deposition technique and time using a three-electrode electrochemical cell. Overall, the impedance of PEDOT:PSS-coated electrodes decreases for all types of electrodes as shown in **Figure 3** for potentiostatic technique and in Figure S7 (Supporting Information) for galvanostatic and CV techniques. As a general trend, the impedance of uncoated electrodes reduces continuously during the coating of PEDOT:PSS with its significant drop at already 5 s of deposition and afterwards its rate slows down. The measured impedance values at this point decrease by 40% (from 70 ± 0.1 to 29.2 ± 0.4 Ω) for m-Au, 98% for μ-Au (from 304 ± 5.4 to 1.73 ± 0.5 kΩ), and 92% (from 124 ± 5.4 to 9.6 ± 0.1 kΩ) in μ-C electrodes at 1 kHz, which is representative frequency in biosignaling[15] (see the Supporting Information for data, Figure S8). Following the systematic monitoring of the electrode surfaces, the maximum PEDOT:PSS thickness attains at different deposition times on three types of electrodes before cracking. As presented in Figure 2 (middle), the PEDOT:PSS covers the entire m-Au electrode's surface at 100 s, μ-Au at 50 s, and μ-C at 75 s of polymerization time. Therefore, from 5 s to higher deposition times the impedance changes at 1 kHz are minor (Figure S7, Supporting Information).

This is also seen in the phase angle evaluation at 1 kHz in all types of electrodes. The phase decreases to lower degrees (from 30° to 70° to below 10°) as shown in Figure 3 and Figure S9 (Supporting Information). Such electrode behavior is largely explained as a resistive.[62] It moves toward frequency dependent at lower frequencies by a progressive raise of impedance magnitude and the phase angle. In contrast, the CV technique shows a different behavior on m-Au with a similar tendency but with a slower progression. This is also remarkable in impedance data, where the magnitude drops dramatically with small variations between the numbers of cycles (Figure S7c, Supporting Information). As discussed above, this observation confirms that the kinetics of the PEDOT:PSS's film growth is slower in the CV technique compared to the potentiostatic and galvanostatic ones. With an increasing deposition time, the thickness of PEDOT:PSS film increases and this is generally reflected on the progressive behavioral shift from higher to lower frequencies of the electrodes. Therefore, the electrodeposition time is the main factor to tune electrochemical properties of the coatings after achieving the first significant reduction of the impedance.

As the electrochemical behavior of electrodes changes with frequency, a cut-off frequency can be defined. Electrode's impedance at frequencies lower than the cut-off frequency (typically above 10 kHz for metal electrodes) increases by a couple of order of magnitudes and the electrode is considered to behave as a capacitor.[9] PEDOT:PSS coating on all types of electrodes lowers the cut-off frequency considerably. It decreases from 1000 ± 25 to 5 ± 0.6 Hz for m-Au electrode and 63 ± 11 Hz for μ-Au electrode. The cut-off frequency of μ-C electrodes decreases to 1.2 ± 0.05 Hz (Figure 3, values are reported in Figure S8, Supporting Information).[15,24,62] Large electrodes have lower cut-off frequency while microelectrodes have cut-off frequency above 10 kHz. PEDOT:PSS coating enlarges the active electrochemical surface of the electrodes allowing for its volumetric capacitance to increase. This delays the formation of double layer capacitance at the interface to lower frequencies. This is critical when it comes to bioelectrical signals transduction. Signals with high frequencies at the interface with low cut-off frequency electrodes attenuate only by the electrodes' resistive behavior in a frequency-independent and non-phase-shifted way. However, electrodes with high cut-off will tend

ADVANCED ELECTRONIC MATERIALS
Open Access
www.advelectronicmat.de

to attenuate signals with different strength and frequency-dependent manner.[15] Therefore, it is important to control the electrodes' impedance and cut-off frequency according to the application.

2.4. Equivalent Circuit Model of PEDOT:PSS Growth

The EIS profiles of PEDOT:PSS growing films allows for modeling their electrochemical and physical characteristics using three types of equivalent circuits (see **Figure 4**).[63] The electrochemical impedance of microelectrodes is typically modeled through the so-called Randles circuit.[38,64,65] It consists of a resistor (R_s) in series with a parallel combination of a capacitor (C_{dl}) and a resistor (R_{ct}) plus a Warburg element (W) (Figure 4a). R_s, is a spread resistivity, representing the resistance against current flow by ion migration which depends on electrode size and interfacing solution resistivity. The parallel circuit is composed of the C_{dl}, the double-layer capacitance, and the faradaic component of the impedance, represented by R_{ct} and W. The appearance of double-layer structure and the faradaic reactions are in parallel as they both take place at the interface between the electrode and the electrolyte. R_{ct} is the charge transfer resistance,[66] while W quantifies the solution species diffusion toward and away from the electrode–electrolyte interface due to a gradient in the ionic concentration. Therefore, W represents the frequency dependence of impedance of the ion transfer at the interface, which appears by 45° slope in phasic (Bode) representation of the impedance.[24,65]

The equivalent circuits, together with SEM observations, allow for structural understanding of the film growth and their electrochemical behavior during the synthesis. The first adopted equivalent circuit model is the Randles circuit, $R_s(C_{dl}(R_{ct}W))$, as reported in Figure 4a,b showing m-Au and µ-Au electrodes surfaces after 5 s of deposition. At this stage only a very thin layer of PEDOT:PSS covers the surface of the electrode that behaves following the Randles circuit.

The second adopted model represents the behavior of the µ-C coated electrode, as shown in Figure 4c and Figure S4 (Supporting Information), at the same deposition time. The surface contains separate islands of PEDOT:PSS that does not fully cover the electrode. Here, for a better fitting, we replaced the W element with a constant phase element (Q) resulting in a $R_s(C_{dl}(R_{ct}Q))$ circuit. Q models the surface irregularities and the interface porosity[67] and it quantifies how close a surface can be to an ideal capacitor [see Equation (1)]. In this case, the rough surface of the electrodes is a predominant factor with respect to the mass transfer represented by the W element.

$$\left(z_Q = \frac{1}{(j\omega)^n} Q_0 \right) \tag{1}$$

where n is the exponent ranging from 0 to 1. Where $n = 1$, the system behaves as an ideal capacitor, while $n = 0$ is a resistor.

Following SEM inspection, the PEDOT:PSS growth reaches a confluent layer after 10 s on µ-Au and 20 s on µ-C electrodes. The recorded impedances follow the third R_sWC_{dl} model at greater deposition times. In µ-Au electrodes, after 10 s, the R_{ct} can be neglected as it reaches as high as the giga-ohm range and at that point, almost no current passes. In this stage, PEDOT:PSS film grows enough to fully cover the electrode surface. It follows the volumetric capacitance evaluation of the PEDOT:PSS which hinders the charge transfer at the interface. In the case of µ-C electrodes, R_{ct} and Q are removed,

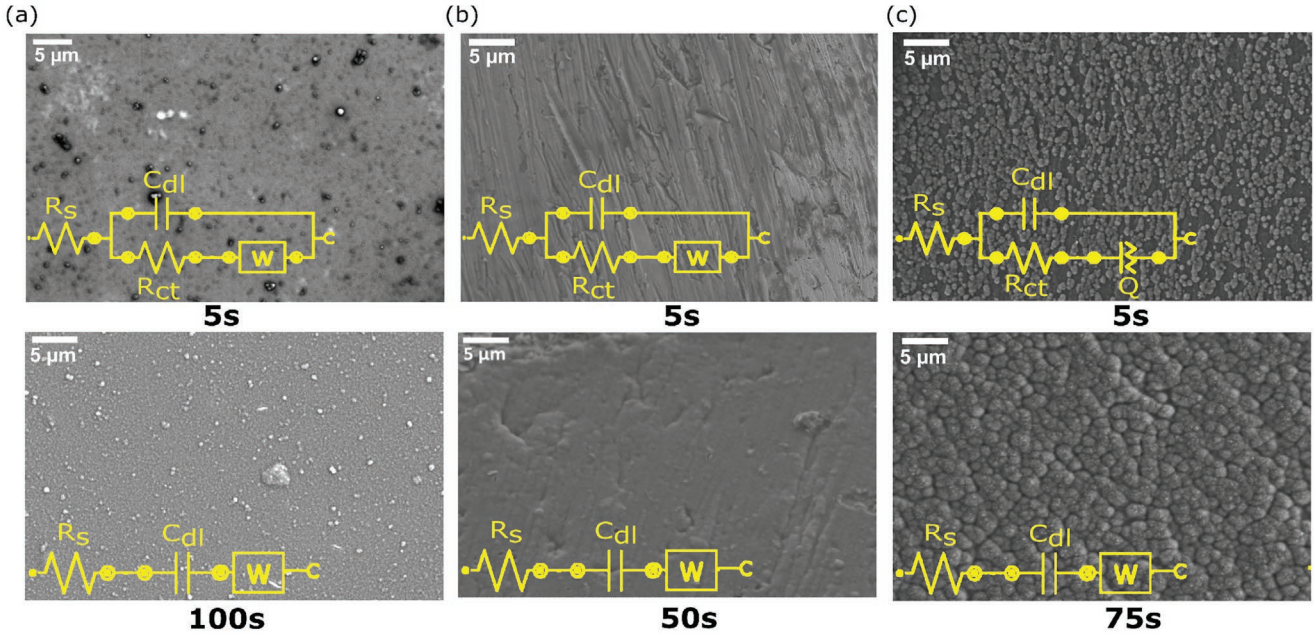

Figure 4. Modeled equivalent circuits of PEDOT:PSS growing films at different times of deposition. SEM image with its equivalent circuit of a) m-Au electrode after 5 s of deposition (top) and after 100 s of deposition (bottom). R_{ct} is removed from the circuit upon coating PEDOT:PSS. b) µ-Au electrode after 5 s of deposition (top) and after 50 s of deposition (bottom). R_{ct} is removed from the circuit upon PEDOT:PSS coating. c) µ-C electrode after 5 s of deposition (top) and after 75 s of deposition (bottom). Q is replaced with W and R_{ct} is removed from the circuit upon coating PEDOT:PSS.

and the circuit is replaced with $R_s WC_{dl}$ after 20 s of deposition. The elimination of Q is attributed to the n value. Up to 20 s, it is 0.96 ± 0.02 while after continuing the deposition for another 30 s it reaches 1. The Warburg element is introduced to the circuit for modeling the diffusion impedance (Figure 4c, bottom). Finite-length Warburg diffusion impedance coefficient [δ ($\Omega S^{-1/2}$)] is calculated from Y_0, the magnitude of the admittance ($1/Z$) at $w = 1$ rad s^{-1} (≈0.16 Hz) [see Equation (2)].

$$\left(\delta = \frac{1}{\gamma_0 \sqrt{2}}\right) \tag{2}$$

The σ value decreases linearly upon PEDOT:PSS growth from 1057 to 33.3 Ω $S^{-1/2}$ for m-Au, from 839 to 11.3 kΩ $S^{-1/2}$ for the µ-Au electrode, and from 4029 to 3.4 kΩ $S^{-1/2}$ for µ-C electrode. The σ drops with PEDOT:PSS thickness increase due to the system transferring to be predominantly resistive behavior.[54]

Here, R_s remains unchanged for all electrodes, independently of PEDOT:PSS coating, as it only depends on the geometry and type of the electrode after the full coverage. C_{dl} increases with deposition time up to 2.64 mF for m-Au, 1.32 µF for µ-Au, and 20 µF for µ-C electrode thanks to volumetric capacitance of PEDOT:PSS with an ability of charge transfer (data resumed in Table S1, Supporting Information). Therefore, the PEDOT:PSS growth causes electrodes to become dominantly resistive to the mass transfer which is proven by W coefficient drop.[66]

These observations are generalized over different electropolymerization techniques, where PEDOT:PSS reduces electrode's impedance already during the first deposition seconds by several orders of magnitude. Therefore, its electrochemical profile changes with time of the deposition until obtaining a fully confluent layer, which depends on the type of the electrode. This deposition time needs to be respected while the coating of electrodes with predominantly resistive or capacitive behaviors.

2.5. Electrochemical Evolution of Film Capacitance and Its Stability

Following the evaluation of the electrochemical behavior of PEDOT:PSS, the progression of the double layer capacitance is measured by the CV technique since it encompasses the charge capacity evolution during the coating. **Figure 5**c shows the plot of the current density (mA m^{-2}) versus the scan rate (V s^{-1}). The slope of this plot represents double-layer capacitance (mF) of the electrode. Figure 5a depicts the m-Au electrodes double-layer capacitance coated for 5, 10, 20, 50, and 100 s. A great correlation between the capacitance calculated from the CV experiment and the values obtained from the equivalent circuit model is reached. For example, C_{dl} for 100 s deposition time is 6.6 F m^{-2}, and it is 8.4 F m^{-2} in an equivalent circuit (**Table 1**). Results in Table 1 show a strong proof of the good compliance of the equivalent circuit adopted at each stage of polymerization to explain how PEDOT:PSS evolves its electrical properties during its growth.

The correlation between the capacitance of the electrodes and the film roughness can be intuitively proposed. The double-layer capacitance of m-Au increases from 0.955 to 6.6 F m^{-2} upon the PEDOT:PSS coating (from 5 to 100 s). This number is almost ten times higher for µ-Au and µ-C where the capacitance changes from 13.5 to 111.6 F m^{-2} (5 to 50 s) and from 21.5 to 281 F m^{-2}, respectively. For example, at 50 s deposition time the capacitance values of m-Au, µ-Au, and µ-C are 4.2, 111.6, and 207 F m^{-2}, respectively. As shown in Figure 2, PEDOT:PSS forms a rougher film on µ-C and µ-Au electrodes. Therefore, PEDOT:PSS forms a flat film on m-Au electrodes. This change of roughness results in a twofold increase of capacitance normalized to the electrode's geometrical surface area for µ-C and µ-Au in comparison with m-Au. This can be due to the stronger adhesion of PEDOT:PSS to initially rough surfaces. Comparing our results with the state of the art, the average capacitance of metal microelectrodes is about 20 µF m^{-2}.[15,67] Therefore, PEDOT:PSS coating increases this number considerably. For example, X. Cui obtained the capacitance of 800 F m^{-2} in PEDOT:PSS gold electrodes.[38] In another study by Wutsoni, PEDOT:PSS-coated electrodes on gold reached the capacitance of 350 F m^{-2},[49] while Chen et al. measured the capacitance of 10.4 F m^{-2}.[68] This general increase of capacitance is due to two mechanisms: volumetric capacitance of PEDOT:PSS and an increase of the active electrochemical surface area of the electrode. Both of those routes are considerably related to the surface structure.[24,69,70]

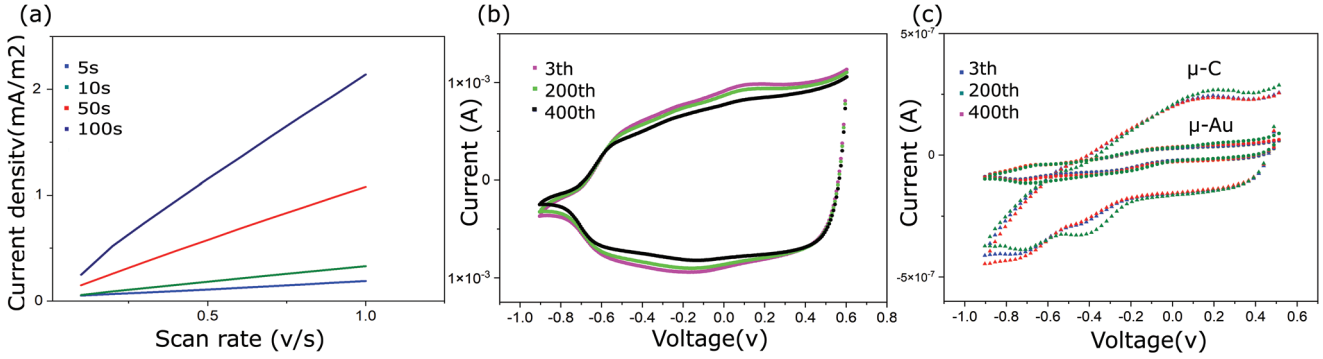

Figure 5. CV measurements. a) Current density of m-Au electrode evaluation at various deposition times against the scan rate. The slope of the line represents the evolving double layer capacitance. Electrochemical stability measurement of b) m-Au electrode and c) µ-Au and µ-C electrodes, over 400 CV scans between –0.9 to +0.6 V with 0.5 V s^{-1}.

Table 1. Comparison of double-layer capacitance (F m^{-2}) of PEDOT:PSS measured by CV technique and the equivalent circuit mode (EC) at various depositions.

Deposition time [s]	5	10	20	50	75	100
m-Au electrode [F m^{-2}]						
CV	0.96	1.91	3.5	4.2	–	6.6
EC	0.73	1.5	2.92	5.8	–	2.64
μ-Au electrode [F m^{-2}]						
CV	13.5	57	65.5	111.6	–	–
EC	11.3	21.1	42.21	99.5	–	–
μ-C electrode [F m^{-2}]						
CV	21.5	45.3	87.5	207	286	–
EC	11.1	27.1	47.9	106.9	159.8	–

In addition to capacitance measurements, CV is used to estimate the electrochemical stability of PEDOT:PSS over oxidation-reduction cycles. Any changes during potential swiping shows structural changes such as film delamination, cracking, or reorganization. Here, m-Au (Figure 5b), μ-Au and μ-C (Figure 5c) electrodes at 100, 50, and 75 s of deposition undergo CV cycles. The potential window includes the reversible redox reaction yet is narrow enough to avoid overoxidation.[37] The CV area and its characteristics does not change after 400 cycles for all electrodes. This indicates the electrochemical stability of the polymer during oxidation-reduction processes in the non-faradaic current window. Cui et al. observed the similar behavior for electropolymerized PEDOT:PSS film.[38] Wustoni performed the same measurement on PEDOT:PSS for 500 cycles and showed 37% reduction of the PEDOT:PSS charge capacity. However, this drop is compared to the first cycle of the CV and, afterward, it conserves its stable redox activity without a considerable drop over 500 cycles.[49] This can be explained by the structure rearrangement of films.[38] The reduction peak for PEDOT:PSS is around –0.7 V for m-Au and μ-Au electrodes and –0.3 V for μ-C electrodes. Even though the adhesion and capacitance of the PEDOT:PSS film is highly affected by the substrate roughness, an optimized electropolymerization ensures the film stability during oxidation/reduction processes.

3. Conclusion

Thanks to its unique properties, in particular mixed ion-electronic conductivity, PEDOT:PSS is frequently used in various applications such as energy conversion, electronic textiles, flexible and stretchable electronics, and bioelectronics. The understanding of PEDOT:PSS electropolymerization allows for optimization and control of the electrical, electrochemical and mechanical properties of electrodes. Our results confirm that during electropolymerization, the ratio of polymerized PEDOT to PSS does not change and the film growth begins at a very early stage. Electrical and optical properties follow the time-dependent behavior with a progressive increase of the PEDOT:PSS film thickness. The potentiostatic technique shows a comparable yet slightly higher sulfur growth kinetics and PEDOT:PSS's film conductivity around 100 ± 7 S cm^{-1} on m-Au supporting electrodes. The relationship between the substrate characteristics and the electrodeposition techniques show that the morphology of PEDOT:PSS and its adhesion to the electrode surface mostly depends on the electrode's surface. PEDOT:PSS forms a cauliflower shape on μ-C electrodes, while it tends to form a flat layer on m-Au and μ-Au electrodes. Slower cracking appearance and their lower size distribution suggest that PEDOT:PSS has better adhesion to μ-C electrodes in comparison with μ-Au electrodes. In terms of electrical performances, PEDOT:PSS coating reduced the impedance by two orders of magnitude already after a few seconds of deposition. Modeled equivalent circuits indicate that electrochemical properties evolve with the time of deposition and allow following the capacitance increase over the film growth. These results highlight the importance in defining the impedimetric profile of the PEDOT:PSS film growth for each type of electropolymerization and for each type of supporting electrode to yield a stable and an efficient coating. Based on presented kinetics of the PEDOT:PSS growth, future studies should focus on the development of molecular dynamics models describing mixed conduction mechanisms in electropolymerized conducting polymers in correlation to their electrochemical properties.

4. Experimental Section

Material: 3,4-Ethylenedioxythiophene (EDOT) and poly(sodium 4-styrenesulfonate) (NaPSS) were purchased from Sigma Aldrich. Carbon-P 2.85 mm diameter filament and gold 0.125 mm diameter wire with polyester insulation were provided by RS component and Goodfellow companies, respectively. Kapton sheets of the 0.125 mm thickness were obtained from Addevmatrial Company. All other chemicals were used as received from Sigma Aldrich.

Electrodes: Three types of electrodes were used as a starting surface for electrodeposition. First, carbon filaments were extruded in a 3D printer (Ultimaker 3) to produce carbon wires (μ-C) of 0.4 mm diameter. They were cut in 2 cm length and cold soldered to the connecting pins. The process was followed by the deposition of 2 μm thick Parylene-C (CSC deposition system PDS-2010) insulator in the presence of a silane adhesion promoter. The electrodes tips were gently wet polished on 2000 silicon paper at 50 rpm using Strure Labopol-5polisher to open the electrodes sites. Second, gold wires (μ-Au) of 0.125 mm diameter insulated by polyester were cut in 2 cm length, washed with isopropanol and the tips were polished with the procedure mentioned above. The third type of electrodes is macro gold electrodes (m-Au). Kapton film was soaked in 1% soap cleaning solution and put in an ultrasonic bath for 15 min, rinsed with isopropanol and dried with nitrogen gas.

The cleaned Kapton was treated with O_2 plasma (Oxford Instruments, Plasmalab 80+) and coated with a 10 nm chromium as adhesion layer and 200 nm gold in a metal evaporator (Boc Edwards, auto 500). Macro electrodes (m-Au) of 1 cm diameter were cut by LPKF, ProtoLaser S laser and rinsed with isopropanol and deionized water.

Electropolymerization: Aqueous solutions of 0.01 M EDOT and 0.1 M NaPSS were prepared under vigorous stirring and purged with nitrogen gas. The electrodeposition took place in a three-electrode cell setup using Metrohm Autolab B.V. potentiostat/galvanostat under potentiostatic (using 1.1 V), galvanostatic (using 0.5 mA cm^{-2}), and cyclic voltammetry technique (–0.6 to 1.1 V with 50 mV s^{-1} scan rate) as described in the following literature.[31,38] The applied current and voltage were set versus the Ag/AgCl reference electrode and a large platinum electrode, used as the counter electrode. Three types of electrodes were used as working electrodes that are presented above.

Electrochemical Impedance Spectroscopy: The impedance measurements were performed in PBS solution in a three-electrode cell setup (Metrohm Autolab B.V.). Platinum wire and Ag/AgCl electrodes were used as the counter and reference electrodes, respectively. The impedance of the three different types PEDOT:PSS-coated electrodes was measured under the constant voltage of 0.01 V versus the reference electrode with sinusoidal waveform between 1 Hz and 10 kHz. Equivalent circuits were modeled on Nova 1.2 software (Metrohm Autolab B.V.).

Cyclic Voltammetry Evaluations: The CV technique is used to evaluate electrochemical stability of PEDOT:PSS coating. Electrodes which were electrodeposited with PEDOT:PSS undergo 400 cycles of CV scans sweep between –0.9 and +0.6 V with 0.5 V s^{-1} scan rate in PBS solution in a three-electrode cell setup.[23] The capacitance of the electrodes upon coating with PEDOT:PSS was also measured via the CV technique. Ten CV scans were applied in the voltage ranging from –0.9 to 0.6 V at various scan rates from 0.1 to 1 V s^{-1}. The double-layer capacitance was measured as the slope of current density versus scan rate and modeled with a linear fit.

PEDOT:PSS/PVA Film Preparation: A 100 µL of 10% (W/W) water solution of PVA was drop casted on the m-Au electrode coated with PEDOT:PSS. The electrode was then dried at room temperature overnight. The PEDOT:PSS film with PVA supporting layer was gently peeled off from the m-Au electrode by applying a small strength at the surface with a tweezer.

Adhesion Force Measurement: To measure the adhesion of the PEDOT:PSS film on m-Au electrodes, the peel-off test was performed. Nylon fiber was placed on the samples followed by PVA (10% W/W) drop casting. Then, the nylon fiber was pulled off from the samples with Instron tensile tester machine (Model: 3365) with the speed of 2 mm min^{-1} until the PEDOT:PSS film was detached. The force measured was reported as the adhesion force. This value was measured around 300 ± 100 mN for different samples.

Four-Point Probe Measurement: Four-point probe (Keithley 2612A) was used to measure the sheet's resistivity and calculate electrical conductivity of PEDOT:PSS from the PEDOT:PSS/PVA film. A current between 0.1 and 1 mA with 0.1 steps was applied through one pair of electrodes and the voltage was recorded using another pair. The resistivity was calculated based on Ohm's law. Since the thickness of the film is considerably smaller than its surface area, the sheet resistivity was obtained according to Equation (3)

$$R_{\text{sheet}} = \frac{V}{I}\frac{\pi}{\ln 2} \tag{3}$$

where R is the electrical resistivity (Ω), V is the voltage (V), I is the current (A), and t is the thickness of the film (cm). The resulting conductivity of the PEDOT:PSS film was obtained from Equation (4) and in S cm^{-1}.

$$\delta = \frac{1}{R_{\text{sheet}} t} \tag{4}$$

UV–Vis Spectroscopy: The transmittance spectrum of PEDOT:PSS on the PVA supporting layer was measured with the UV–vis spectrophotometer (Shimadzu UV-2600). The film was fixed in the sample holder and the spectra were obtained between 200 and 1400 nm.

FTIR Spectroscopy: ATR mode was used to measure the FTIR spectrum of PEDOT:PSS/PVA film with Shimadzu IRAFFINITY-1S. It allows the direct measurement of the infrared transmission spectra of films.

Raman Spectroscopy: The spectra of PEDOT:PSS on m-Au electrodes were measured using the Horiba Jobin-Yvon machine (Model: LabRAM-HR) with 785 nm laser excitation. Peaks were found using Gaussian fit.

Scanning Electron Microscopy: The secondary electron detector (SE) and EDX sensor were used to investigate the electrode's structure before and after coating with PEDOT:PSS using Carl Zeiss Ultra55. All images were taken at 5 kV voltage. The thickness of PEDOT:PSS film on PVA was measured while samples were tilted at 90° position from the cross-section images. These measurements were performed on the synthesized film with potentiostatic technique at 5–200 s deposition times.

Supporting Information

Supporting Information is available from the Wiley Online Library or from the author.

Acknowledgements

This work was supported by the French National Research Agency through the ANR JCJC OrgTex project (ANR-17-CE19-0010) and ANR NEURO-SENSE project (ANR-18-CE19-0013). E.I. wishes to thank CMP cleanroom staff at the Center of Microelectronics in Provence for their technical support during the development of the project.

Conflict of Interest

The authors declare no conflict of interest.

Data Availability Statement

The data that support the findings of this study are available from the corresponding author upon reasonable request.

Keywords

electropolymerization, impedance, organic electronics, PEDOT:PSS, thin films

Received: December 5, 2022
Revised: February 13, 2023
Published online: April 21, 2023

[1] J. Rivnay, R. M. Owens, G. G. Malliaras, *Chem. Mater.* **2014**, *26*, 679.
[2] J. Rivnay, M. Ramuz, P. Leleux, A. Hama, M. Huerta, R. M. Owens, *Appl. Phys. Lett.* **2015**, *106*, 043301.
[3] A. Williamson, M. Ferro, P. Leleux, E. Ismailova, A. Kaszas, T. Doublet, P. Quilichini, J. Rivnay, B. Rõzsa, G. Katona, C. Bernard, G. G. Malliaras, *Adv. Mater.* **2015**, *27*, 4405.
[4] D. Khodagholy, T. Doublet, P. Quilichini, M. Gurfinkel, P. Leleux, A. Ghestem, E. Ismailova, T. Hervé, S. Sanaur, C. Bernard, G. G. Malliaras, *Nat. Commun.* **2013**, *4*, 1575.

[5] M. Galliani, L. M. Ferrari, E. Ismailova, *Biosensors* **2022**, *12*, 305.
[6] L. M. Ferrari, S. Sudha, S. Tarantino, R. Esposti, F. Bolzoni, P. Cavallari, C. Cipriani, V. Mattoli, F. Greco, *Adv. Sci.* **2018**, *5*, 1700771.
[7] S. Takamatsu, T. Lonjaret, D. Crisp, J. M. Badier, G. G. Malliaras, E. Ismailova, *Sci. Rep.* **2015**, *5*, 15003.
[8] C. J. Bettinger, M. Ecker, T. D. Y. Kozai, G. G. Malliaras, E. Meng, W. Voit, *MRS Bull.* **2020**, *45*, 655.
[9] J. T. Robinson, E. Pohlmeyer, M. C. Gather, C. Kemere, J. E. Kitching, G. G. Malliaras, A. Marblestone, K. L. Shepard, T. Stieglitz, C. Xie, *IEEE Sens. J.* **2019**, *19*, 10163.
[10] M. Bianchi, A. De Salvo, M. Asplund, S. Carli, M. Di Lauro, A. Schulze-bonhage, T. Stieglitz, L. Fadiga, F. Biscarini, *Adv. Sci.* **2022**, *1*, 2104701.
[11] J. Rivnay, S. Inal, B. A. Collins, M. Sessolo, E. Stavrinidou, X. Strakosas, C. Tassone, D. M. Delongchamp, G. G. Malliaras, *Nat. Commun.* **2016**, *7*, 11287.
[12] B. D. Paulsen, K. Tybrandt, E. Stavrinidou, J. Rivnay, *Nat. Mater.* **2020**, *19*, 13.
[13] K. A. Ludwig, J. D. Uram, J. Yang, D. C. Martin, D. R. Kipke, *J. Neural Eng.* **2006**, *3*, 59.
[14] S. Savagatrup, E. Chan, S. M. Renteria-Garcia, A. D. Printz, A. V. Zaretski, T. F. O'Connor, D. Rodriquez, E. Valle, D. J. Lipomi, *Adv. Funct. Mater.* **2015**, *25*, 427.
[15] C. Boehler, S. Carli, L. Fadiga, T. Stieglitz, M. Asplund, *Nat. Protoc.* **2020**, *15*, 3557.
[16] K. D. Harris, R. Q. Quiroga, J. Freeman, S. L. Smith, *Nat. Neurosci.* **2016**, *19*, 1165.
[17] X. Liu, A. Demosthenous, N. Donaldson, *Med. Biol. Eng. Comput.* **2008**, *46*, 997.
[18] V. Viswam, M. E. J. Obien, F. Franke, U. Frey, A. Hierlemann, *Front. Neurosci.* **2019**, *13*, 385.
[19] Z. Aqrawe, J. Montgomery, J. Travas-Sejdic, D. Svirskis, *Sens. Actuators, B* **2018**, *257*, 753.
[20] M. J. Nelson, P. Pouget, E. A. Nilsen, C. D. Patten, J. D. Schall, *J. Neurosci. Methods* **2008**, *169*, 141.
[21] G. Buzsáki, *Nat. Neurosci.* **2004**, *7*, 446.
[22] G. Buzsáki, *Rhythms of the Brain*, Oxford University Press, New York **2009**.
[23] G. Tarabella, N. Coppedè, S. Iannotta, F. Cicoira, P. Kumar, C. Santato, *Handbook of Organic Materials for Optical and (Opto) Electronic Devices: Properties and Applications*, **2013**, p. 597.
[24] X. Cui, J. F. Hetke, J. A. Wiler, D. J. Anderson, D. C. Martin, *Sens. Actuators, A* **2001**, *93*, 8.
[25] G. Dijk, H. J. Ruigrok, R. P. O'Connor, *Adv. Mater. Interfaces* **2020**, *7*, 2000675.
[26] M. Berggren, G. G. Malliaras, *Science* **2019**, *364*, 233.
[27] M. J. Donahue, A. Sanchez-Sanchez, S. Inal, J. Qu, R. M. Owens, D. Mecerreyes, G. G. Malliaras, D. C. Martin, *Mater. Sci. Eng., R* **2020**, *140*, 100546.
[28] A. Sanchez-Sanchez, I. del Agua, G. G. Malliaras, D. Mecerreyes, *Conductive Poly(3,4-ethylenedioxythiophene) (PEDOT)-Based Polymers and Their Applications in Bioelectronics*, 2nd ed., Elsevier, Amsterdam **2019**.
[29] E. Zeglio, A. L. Rutz, T. E. Winkler, G. G. Malliaras, A. Herland, *Adv. Mater.* **2019**, *31*, 1806712.
[30] R. Kiebooms, A. Aleshin, K. Hutchison, F. Wudl, A. Heeger, *Synth. Met.* **1999**, *101*, 436.
[31] Y. Vlamidis, M. Lanzi, E. Salatelli, I. Gualandi, B. Fraboni, L. Setti, D. Tonelli, *J. Solid State Electrochem.* **2015**, *19*, 1685.
[32] K. Sun, S. Zhang, P. Li, Y. Xia, X. Zhang, D. Du, F. H. Isikgor, J. Ouyang, *J. Mater. Sci.* **2015**, *26*, 4438.
[33] H. Yamato, K. I. Kai, M. Ohwa, W. Wernet, M. Matsumura, *Electrochim. Acta* **1997**, *42*, 2517.
[34] H. Yamato, M. Ohwa, W. Wernet, *J. Electroanal. Chem.* **1995**, *397*, 163.
[35] Z. U. Khan, O. Bubnova, M. J. Jafari, R. Brooke, X. Liu, R. Gabrielsson, T. Ederth, D. R. Evans, J. W. Andreasen, M. Fahlman, X. Crispin, *J. Mater. Chem. C* **2015**, *3*, 10616.
[36] V. Castagnola, E. Descamps, A. Lecestre, L. Dahan, J. Remaud, L. G. Nowak, C. Bergaud, *Biosens. Bioelectron.* **2015**, *67*, 450.
[37] V. Castagnola, C. Bayon, E. Descamps, C. Bergaud, *Synth. Met.* **2014**, *189*, 7.
[38] X. Cui, D. C. Martin, *Sens. Actuators, B* **2003**, *89*, 92.
[39] R. A. Green, R. T. Hassarati, L. Bouchinet, C. S. Lee, G. L. M. Cheong, J. F. Yu, C. W. Dodds, G. J. Suaning, L. A. Poole-Warren, N. H. Lovell, *Biomaterials* **2012**, *33*, 5875.
[40] C. K. Cho, W. J. Hwang, K. Eun, S. H. Choa, S. I. Na, H. K. Kim, *Sol. Energy Mater. Sol. Cells* **2011**, *95*, 3269.
[41] L. Ouyang, B. Wei, C.-C. Kuo, S. Pathak, B. Farrell, D. C. Martin, *Sci. Adv.* **2017**, *3*, 1600448.
[42] J. Qu, N. Garabedian, D. L. Burris, D. C. Martin, *J. Mech. Behav. Biomed. Mater.* **2019**, *100*, 103376.
[43] C. Boehler, F. Oberueber, S. Schlabach, T. Stieglitz, M. Asplund, *ACS Appl. Mater. Interfaces* **2017**, *9*, 189.
[44] B. Wei, J. Liu, L. Ouyang, C. C. Kuo, D. C. Martin, *ACS Appl. Mater. Interfaces* **2015**, *7*, 15388.
[45] E. J. Welle, J. E. Woods, A. A. Jiman, J. M. Richie, E. C. Bottorff, Z. Ouyang, J. P. Seymour, P. R. Patel, T. M. Bruns, C. A. Chestek, *bioRxiv* **2021**, *29*, 993.
[46] I. M. Taylor, N. A. Patel, N. C. Freedman, E. Castagnola, X. T. Cui, *Anal. Chem.* **2019**, *91*, 12917.
[47] X. Yang, J. Kirsch, E. V. Olsen, J. W. Fergus, A. L. Simonian, *Sens. Actuators, B* **2013**, *177*, 659.
[48] J. Heinze, A. Rasche, M. Pagels, B. Geschke, *J. Phys. Chem. B* **2007**, *111*, 989.
[49] S. Wustoni, A. Saleh, J. K. El-Demellawi, A. Koklu, A. Hama, V. Druet, N. Wehbe, Y. Zhang, S. Inal, *APL Mater.* **2020**, *8*, 121105.
[50] J. Wan, X. Fan, H. Huang, J. Wang, Z. Zhang, J. Fang, F. Yan, *J. Mater. Chem. A* **2020**, *8*, 21007.
[51] M. Modarresi, I. Zozoulenko, *Phys. Chem. Chem. Phys.* **2022**, *24*, 22073.
[52] W. Zhang, B. Zhao, Z. He, X. Zhao, H. Wang, S. Yang, H. Wu, Y. Cao, *Energy Environ. Sci.* **2013**, *6*, 1956.
[53] A. Håkansson, S. Han, S. Wang, J. Lu, S. Braun, M. Fahlman, M. Berggren, X. Crispin, S. Fabiano, *J. Polym. Sci., Part B: Polym. Phys.* **2017**, *55*, 814.
[54] L. Zhang, K. Yang, R. Chen, Y. Zhou, S. Chen, Y. Zheng, M. Li, C. Xu, X. Tang, Z. Zang, K. Sun, *Adv. Electron. Mater.* **2020**, *6*, 1900648.
[55] Y. Seki, M. Takahashi, M. Takashiri, **2019**, *9*, 15957.
[56] M. Kong, M. Garriga, J. S. Reparaz, M. I. Alonso, *ACS Omega* **2022**, *7*, 39429.
[57] W. W. Chiu, J. Travaš-Sejdić, R. P. Cooney, G. A. Bowmaker, *J. Raman Spectrosc.* **2006**, *37*, 1354.
[58] C. Boehler, F. Oberueber, T. Stieglitz, M. Asplund, *Proc. Annu. Int. Conf. IEEE Eng. Med. Biol. Soc. EMBS* **2017**, *49*, 1058.
[59] C. Boehler, D. M. Vieira, U. Egert, M. Asplund, *ACS Appl. Mater. Interfaces* **2020**, *12*, 14855.
[60] C. Boehler, Z. Aqrawe, M. Asplund, *Bioelectron. Med.* **2019**.
[61] G. Nikiforidis, S. Wustoni, C. Routier, A. Hama, A. Koklu, A. Saleh, N. Steiner, V. Druet, H. Fiumelli, S. Inal, *Macromol. Biosci.* **2020**, *20*, 2000215.
[62] G. Massobrio, S. Martinoia, P. Massobrio, *IEEE Trans. Biomed. Circuits Syst.* **2018**, *12*, 3.
[63] S. A. Spanninga, D. C. Martin, Z. Chen, *J. Phys. Chem. C* **2010**, *114*, 14992.
[64] C. M. Proctor, J. Rivnay, G. G. Malliaras, *J. Polym. Sci., Part B: Polym. Phys.* **2016**, *54*, 1433.
[65] M. R. Abidian, D. C. Martin, *Biomaterials* **2008**, *29*, 1273.

[66] N. Lago, A. Cester, N. Wrachien, M. Natali, S. D. Quiroga, S. Bonetti, M. Barbato, A. Rizzo, E. Benvenuti, V. Benfenati, M. Muccini, S. Toffanin, G. Meneghesso, *Org. Electron. Phys., Mater. Appl.* **2016**, *35*, 176.
[67] D. W. Kumsa, N. Bhadra, E. M. Hudak, S. C. Kelley, D. F. Untereker, J. T. Mortimer, *J. Neural Eng.* **2016**, *13*.
[68] S. Chen, W. Pei, Q. Gui, R. Tang, Y. Chen, S. Zhao, H. Wang, H. Chen, *Sens. Actuators, A* **2013**, *193*, 141.
[69] J. Yang, D. C. Martin, *Sens. Actuators, A* **2004**, *113*, 204.
[70] D. A. Koutsouras, P. Gkoupidenis, C. Stolz, V. Subramanian, G. G. Malliaras, D. C. Martin, *ChemElectroChem* **2017**, *4*, 2321.